Rotational alignments in ^{235}Np and the possible role of $j_{15/2}$ neutrons

A. M. Hurst,[1,*] C. Y. Wu,[1] M. A. Stoyer,[1] D. Cline,[2] A. B. Hayes,[2] S. Zhu,[3] M. P. Carpenter,[3] K. Abu Saleem,[4] I. Ahmad,[3] J. A. Becker,[1] C. J. Chiara,[3,5,6] J. P. Greene,[3] R. V. F. Janssens,[3] T. L. Khoo,[3] F. G. Kondev,[3,5] T. Lauritsen,[3] C. J. Lister,[3] G. Mukherjee,[7] S. V. Rigby,[8] D. Seweryniak,[3] and I. Stefanescu[3,6]

[1]*Lawrence Livermore National Laboratory, Livermore, California 94550, USA*
[2]*Department of Physics and Astronomy, University of Rochester, Rochester, New York 14627, USA*
[3]*Physics Division, Argonne National Laboratory, Argonne, Illinois 60439, USA*
[4]*Department of Physics, University of Jordan, Amman 11942, Jordan*
[5]*Nuclear Engineering Division, Argonne National Laboratory, Argonne, Illinois 60439, USA*
[6]*Department of Chemistry and Biochemistry, University of Maryland, College Park, Maryland 20742, USA*
[7]*Variable Energy Cyclotron Centre, 1/AF Bidhan Nagar, Kolkata-700 064, India*
[8]*Oliver Lodge Laboratory, University of Liverpool, Liverpool L69 7ZE, United Kingdom*

(Received 9 September 2009; published 22 January 2010)

The role $j_{15/2}$ neutron orbitals play in the transuranic region of actinides has been studied by exploring γ-ray transitions between yrast states in ^{235}Np, populated utilizing the nucleon-transfer reaction ^{237}Np(^{116}Sn,^{118}Sn). Two rotational sequences, presumably the two signatures of the ground-state band, have been delineated to high spin for the first time, with the $\alpha = +1/2$ and $\alpha = -1/2$ signature partners reaching $49/2^+\,\hbar$ (tentatively $53/2^+\,\hbar$) and $47/2^+\,\hbar$ (tentatively $51/2^+\,\hbar$), respectively. Definite isotopic assignments for these in-band transitions were established through γ-ray cross correlations between ^{235}Np and ^{118}Sn and events where at least three γ rays corresponding to neptunium-like particles were detected. These transitions reveal clear upbends in the aligned angular momentum and kinematic moment of inertia plots; such a phenomenon could indicate a strong interaction between an aligned $\nu j_{15/2}$ configuration crossing the ground-state band in ^{235}Np, which is based on a $\pi i_{13/2}$ orbital. However, the lack of any signature splitting over the observed frequency range of the ^{235}Np rotational sequences cannot remove the possibility of a $\pi h_{9/2}$ assignment for the observed band. The role of the $\nu j_{15/2}$ and $\pi i_{13/2}$ alignment mechanisms in the deformed U-Pu region is discussed in light of the current spectroscopic data and in the context of the cranked-shell model.

DOI: 10.1103/PhysRevC.81.014312 PACS number(s): 21.10.Re, 23.20.Lv, 25.70.Hi, 27.90.+b

I. INTRODUCTION

The cranked-shell model (CSM), developed by Inglis [1], has achieved remarkable success in providing a microscopic description of single-particle behavior, modified through collective nuclear rotation. The principal success of this model is attributed to its ability to successfully describe the backbending phenomenon [2,3] in terms of a band crossing between the ground-state band and a band based on a rotationally-aligned quasiparticle pair. This interpretation is manifested through the Coriolis interaction, contrary to earlier conjecture citing a collapse in pairing [4]. An additional facet of the model is the description of the oscillatory strong-weak cycling in interaction strength as a function of nucleon number that was first observed in accordance with $i_{13/2}$ neutron-shell filling in the rare-earth region [2,5]. In the rare-earth region where the CSM was first successfully applied, the aligning pairs are either proton $(\pi)\, h_{11/2}$ or neutron $(\nu)\, i_{13/2}$ configurations. These band crossings occur at distinct rotational frequencies depending on whether a proton- or neutron-based configuration is involved.

The backbending phenomenon has also been observed in the deformed transuranic (U-Pu) region, where both the $\pi i_{13/2}$ and $\nu j_{15/2}$ orbitals are located in the vicinity of the Fermi surface and, thus, both proton- and neutron-based orbitals could, in principle, be attributed to any observed alignment effects. This matter is further complicated since the crossing frequency in this region is expected to be similar for rotationally-aligned bands based on either configuration [3,6]. Experimentally, this region is difficult to investigate to high spins due to the limited availability of actinide targets and difficulties in accessing many of these nuclei through standard experimental techniques such as fusion-evaporation reactions owing to their fissile nature. As a result, only select information has been obtained, and accordingly, the alignment mechanism of the high-j orbitals for many of the actinides remains an open question.

The first direct evidence for rotational alignment of the $i_{13/2}$ protons in the actinides was established from g-factor measurements of the high-spin yrast states in the even-even nuclides ^{232}Th and ^{238}U [7], though indirect evidence for the $i_{13/2}$ proton alignment in ^{232}Th [8] and ^{238}U [9] had earlier been established through Coulomb excitation. In addition, the first observation of backbending in an actinide nucleus, and subsequent microscopic interpretation, was reported for proton-aligned $i_{13/2}$ bands in ^{242,244}Pu [10]. Rotationally-aligned $\pi i_{13/2}$ band crossings have also been reported elsewhere from inelastic-scattering measurements in ^{238}U [11], in addition to the lighter even-even uranium isotopes ^{234,236}U [12], and ^{248}Cm [13].

More recently, many of these same nuclei have been reinvestigated using large γ-ray array spectrometers such as

*hurst10@llnl.gov

Gammasphere. For example, recent work on the ^{242,244}Pu isotopes [14] reveals a sharp alignment gain of $\sim 10\ \hbar$ and has been attributed to the alignment of the $i_{13/2}$ protons [10,15,16]. However, this sharp backbending feature has not been observed over the same frequency range in the lighter ^{238,239,240}Pu isotopes. In the latter three cases, there is a significant delay in the alignment process, which could be a consequence of enhanced octupole correlations [14,17,18]. The dominant role of the $i_{13/2}$ proton alignment was also established in ^{235}U and ^{237}Np following an investigation by Kulessa *et al.* [19], while any interaction strength from the $j_{15/2}$ neutron orbitals was reported to be weak. Furthermore, from a systematic study of the high-spin states in the actinides using inelastic scattering [20,21], it has been reported that any contribution to the alignment process due to the $j_{15/2}$ neutron pair is much smaller than expected according to the CSM. Hitherto, no case for a strong interaction based on a $\nu j_{15/2}$ alignment has been identified in the deformed U-Pu region which appears to be at odds with the CSM predictions.

This work aims to achieve a better understanding of the $j_{15/2}$ neutron-alignment mechanism in the U-Pu actinide region by investigating the spectroscopy of ^{235}Np from a two-neutron transfer measurement in order to search for first evidence of a pair of $j_{15/2}$ neutrons strongly contributing to the alignment process in the region.

II. EXPERIMENT AND DATA ANALYSIS

A beam of $^{116}Sn^{31+}$ ions with an intensity of $\sim$0.65 pnA was delivered by the Argonne Tandem-Linac Accelerator System (ATLAS) at Argonne National Laboratory. The beam was incident upon a 0.3-mg/cm^2 thick Ni foil at a beam energy of 801 MeV. A radioactive layer of ^{237}Np ($T_{1/2} = 2.14 \times 10^6$ yr) of thickness 0.5 mg/cm^2 was electroplated onto the downstream side of the Ni foil and covered by a 20-μg/cm^2 thick C layer in order to minimize the possibility of contamination of the experimental equipment through the release of radioactive target material. Following energy loss in the Ni foil, the beam was delivered to the ^{237}Np target with an energy $\sim$20% above the Coulomb barrier. Deexcitation γ rays were detected by the Gammasphere spectrometer [22], a 4π array of 101 Compton-suppressed high-purity germanium (HPGe) detectors, in coincidence with recoiling particles recorded in CHICO, which is a segmented parallel-plate avalanche counter (PPAC) [23]. The CHICO detector is a 4π position-sensitive avalanche counter comprising 20 segmented anodes; it is divided into two hemispheres, forward and backward, covering a polar laboratory range from $12^\circ < \theta < 85^\circ$ and $95^\circ < \theta < 168^\circ$, respectively. However, only the forward hemisphere was used for particle detection in this experiment. A master-trigger requirement of two particles and two γ rays (p-p-γ-γ) firing in prompt coincidence was imposed upon the data-acquisition system in order for events to be written to disk. Approximately 1.7×10^8 coincidence events were collected over the four-day running period.

The data analysis described in this work was performed using software packages based on ROOT [24] and RADWARE [25] codes specifically adapted to meet the needs of Gammasphere experiments and to process the energy, position, and timing information of the recorded particle and γ-ray events. The analysis was based on the construction of coincidence γ-γ matrices and γ-γ-γ cubes that were created under specific sorting constraints. By constructing γ-γ matrices it was possible to confirm the association of previously unknown γ-ray transition energies in ^{235}Np by cross correlating the observed transitions with the known $2_1^+ \rightarrow 0_{\text{g.s.}}^+$ transition at 1230 keV in ^{118}Sn (the $2n$-transfer product). The longest γ-ray cascades in ^{235}Np were then identified by creating γ-γ-γ cubes and projecting triple- and higher-order coincidence background-subtracted spectra, allowing for the weakest members of the cascades to be uncovered. Particle-γ coincidence timing was used to ensure proper selection of prompt γ-ray coincidences, as illustrated in Fig. 1(a). To generate and examine the aforementioned coincidence matrices and cubes, CHICO was used to select coplanar kinematically-coincident particles with a $\frac{\Delta M}{M}$ mass resolution of $\sim$5% [23]. The kinematic separation of projectile-like (Sn) and target-like (Np) events through their

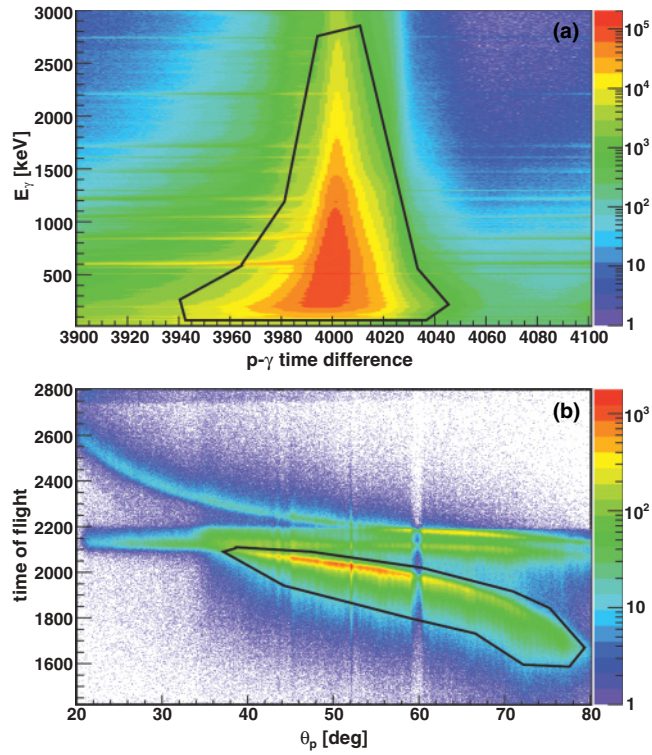

FIG. 1. (Color online) (a) Two-dimensional coincidence timing spectrum illustrating the γ-ray energy vs the particle-γ time difference. The calibration constant for the time axis is $\sim$0.55 ns/channel. The solid black line illustrates the two-dimensional cut used to ensure proper selection of prompt-coincident events in the data analysis. (b) Two-dimensional spectrum showing particle time-of-flight difference vs polar laboratory angle recorded by a CHICO anode in the left-sided hemisphere with respect to the beam direction. The different kinematic tracks allow for separation of projectile-like (Sn) and target-like (Np) species. The solid black line shows an example of a two-dimensional cut used in the analysis to ensure proper selection of projectile-like events.

difference in time-of-flight as a function of polar laboratory angle enabled isotopic identification [see Fig. 1(b)]. Two-dimensional gating was used throughout the analysis to ensure proper selection of the desired projectile range.

III. RESULTS

The signature transitions for the inelastic- and quasielastic-transfer processes observed in this measurement are shown in the coincidence γ-ray spectrum in Fig. 2. This projection of γ rays has been Doppler corrected according to the velocity of tin-like species. The strong peak at 1294 keV corresponds to the $2_1^+ \rightarrow 0_{\text{g.s.}}^+$ transition in ^{116}Sn, observed because of the inelastic scattering of the beam. The signatures for the $1n$- and $2n$-pickup channels can be identified by the $3/2_1^+ \rightarrow 1/2_{\text{g.s.}}^+$ transition at 159 keV in ^{117}Sn and the $2_1^+ \rightarrow 0_{\text{g.s.}}^+$ transition at 1230 keV in ^{118}Sn, respectively. Figure 3 displays the variation in transition intensity as a function of scattering

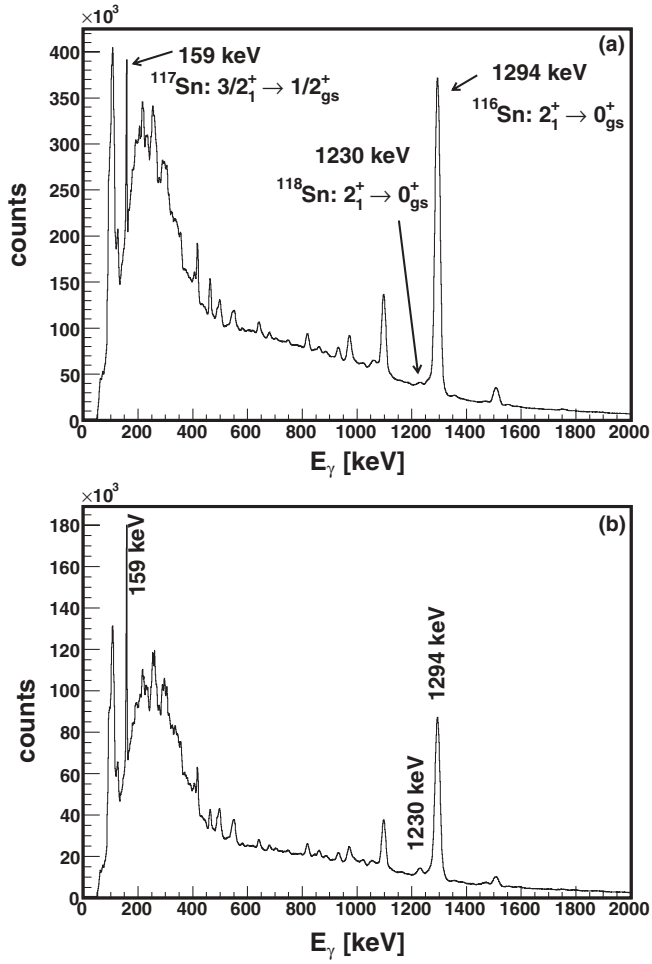

FIG. 2. Coincidence γ-ray energy spectra observed in this experiment revealing the signature transitions for the inelastic- and quasielastic-reaction channels. (a) Total projection p-p-γ-γ coincidence spectrum, Doppler corrected for tin-like species. (b) Same coincidence spectrum gated on a projectile-scattering range of $55^\circ \leqslant \theta_p \leqslant 78^\circ$.

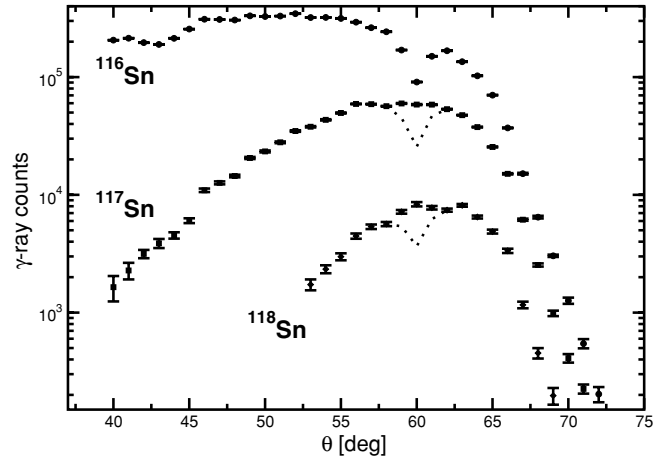

FIG. 3. Logarithmic plot showing the laboratory-frame angular distribution of γ-ray yields for the inelastic channel in addition to the one- and two-neutron pickup channels for the reaction ^{237}Np + ^{116}Sn. The inelastic ^{237}Np(^{116}Sn,^{116}Sn*), one-neutron transfer ^{237}Np(^{116}Sn,^{117}Sn), and two-neutron transfer ^{237}Np(^{116}Sn,^{118}Sn) channels are all labeled. The intensities of the $2_1^+ \rightarrow 0_{\text{g.s.}}^+$ transitions in ^{116}Sn and ^{118}Sn at 1294 and 1230 keV, respectively, were measured as a function of projectile-like laboratory angle in the CHICO, in addition to the $3/2_1^+ \rightarrow 1/2_{\text{g.s.}}^+$ transition at 159 keV in ^{117}Sn. The dip in efficiency at approximately 59°–61° in the ^{116}Sn data is caused by the location of the aluminum rib on the CHICO. This efficiency loss was corrected for in the ^{117,118}Sn data, while the uncorrected efficiencies for these channels are shown by the dotted lines.

angle for the inelastic- and quasielastic-reaction channels observed in this experiment. The most distinct feature for quasielastic, few-nucleon transfer reactions between heavy ions is a bell-shaped angular distribution for the reaction cross section [26]. Indeed, the plot of Fig. 3 reveals such a distribution and effectively indicates that the neutron-transfer cross section rises rapidly with increasing laboratory angle. This can be attributed to an increase in transfer probability as the internucleus distance decreases with increasing scattering angle. The sharp falloff at even larger scattering angles (for all three channels) is caused by the other competing reaction channels that open up when there is a significant overlap between the two reaction partners. The cross sections peak around the grazing angles in the neutron-transfer processes at ∼60° in the ^{237}Np(^{116}Sn,^{117}Sn) one-neutron channel and at ∼63° in the ^{237}Np(^{116}Sn,^{118}Sn) two-neutron channel.

The results from the angular-distribution measurements indicate that enhanced selectivity of the neutron-pickup channels relative to the dominant inelastic branch can be achieved by constructing coincidence γ-γ matrices and γ-γ-γ cubes gated on specific projectile-scattering angles. Indeed, the projectile requirement of $55^\circ \leqslant \theta_p \leqslant 78^\circ$ on the coincidence spectrum in Fig. 2(b) illustrates the case. Both the $1n$- and $2n$-transfer channels show, respectively, threefold and fivefold relative enhancements in the corresponding yield of the signature γ-ray transition over the inelastic branch. An asymmetric-coincidence γ-γ matrix (γ-ray energy with a neptunium-like Doppler correction versus γ-ray energy with a tin-like Doppler correction) with the aforementioned projectile

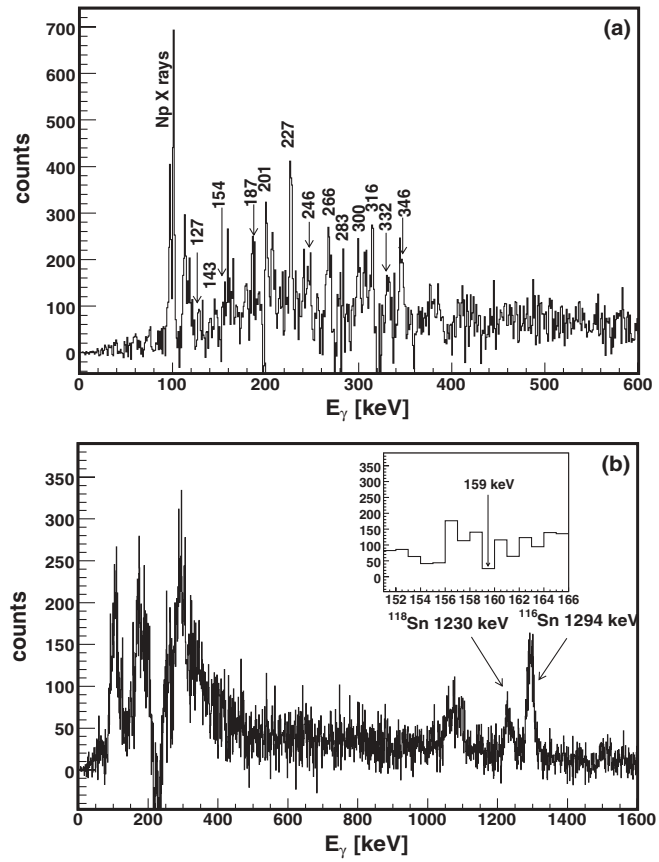

FIG. 4. Doppler-corrected γ-ray spectra: (a) Neptunium-like projection of γ rays in coincidence with the 1230-keV transition in ^{118}Sn. Thirteen new transitions in the $2n$-transfer channel have been identified and labeled. (b) Tin-like projection of γ rays in coincidence with the 227-keV transition observed in the $2n$-transfer channel. The $2^+_1 \rightarrow 0^+_{\text{g.s.}}$ transition in ^{118}Sn at 1230 keV, in addition to the same transition at 1294 keV in ^{116}Sn, is evident. The inset shows the same tin-like projection expanded around the low-energy region. There is no evidence for a transition at 159 keV which would correspond to the $3/2^+_1 \rightarrow 1/2^+_{\text{g.s.}}$ transition in ^{117}Sn in the $1n$-transfer channel.

condition was thus created in order to identify transitions belonging to ^{235}Np, the $2n$-transfer product. By placing a narrow gate around the 1230-keV transition on the tin-like axis, the corresponding projection of γ rays in Fig. 4(a) was observed. Around 13 new transitions can be identified in this projection. However, due to the near-degenerate nature of many γ lines in the actinide nuclei [27], it is imperative to firmly establish unique transitions by cross correlating postulated assignments with known transitions in their corresponding transfer partners. The strongest transition in the spectrum in Fig. 4(a) occurs at 227 keV and was, therefore, used to establish a cross correlation with ^{118}Sn in the $2n$-pickup channel. A narrow gate around 227 keV was imposed on the neptunium-like Doppler-corrected projection of the asymmetric coincidence matrix producing the spectrum of Fig. 4(b). This spectrum reproduces the signature $2^+_1 \rightarrow 0^+_{\text{g.s.}}$ transition at 1230 keV belonging to ^{118}Sn, and thus confirms the ^{235}Np assignment for the spectrum of γ rays observed in Fig. 4(a). The $1n$-transfer product, ^{236}Np, can be ruled out since there is no cross correlation with the 159-keV transition in ^{117}Sn; there is no evidence for this transition in the spectrum shown in Fig. 4(b). It is, however, impossible to completely suppress any contribution from the inelastic branch owing to its overwhelming dominance of the reaction cross section. Furthermore, the 1294-keV transition in ^{116}Sn persists in Fig. 4(b) (in addition to the $4^+_1 \rightarrow 2^+_1$ transition at 1097 keV) due to the presence of a 229-keV transition in the ground-state band of ^{237}Np [20], which is close in energy to the cross-correlated gating transition at 227 keV.

A γ-γ-γ coincidence cube, gated on projectile angles $55^\circ \leqslant \theta_p \leqslant 78^\circ$, was then constructed to provide enhanced selectivity of transitions belonging to the $2n$-transfer channel (observed in the γ-γ matrix analysis). The corresponding level scheme for ^{235}Np from the data collected in this work—the first high-spin study of this nucleus—is proposed in Fig. 5. The presumed ground-state signature partner bands, labeled 1 and 2 in the level scheme, have been newly identified. The corresponding transition energies from this level scheme are also listed in Table I, together with the proposed spin-parity assignments for the transitions involved.

To understand the underlying structure of the observed band in ^{235}Np, the spectroscopic characteristics of this band are compared with the population mechanisms of the π-based bands in ^{237}Np. The γ-γ-γ projection with a neptunium-like Doppler correction in Fig. 6 indicates that the ground-state band of $i_{13/2}$ parentage in ^{237}Np is more intensely populated than the excited $h_{9/2}$ quasiproton band in this nucleus (see proposed ^{237}Np level scheme in Ref. [20]). The intensities of the $33/2 \rightarrow 29/2$ transition in both the $i_{13/2}$ and $h_{9/2}$ bands belonging to ^{237}Np were measured by double-gating on the two members of each cascade directly beneath this transition. These transitions

TABLE I. Transition energies and spin-parity assignments corresponding to the level scheme deduced for ^{235}Np in this work. The uncertainty in E_γ ranges from approximately 0.5 to 1 keV; the strong γ rays have the least uncertainty, while the larger uncertainty is associated with the weaker transitions. Spin-parity values are presented under the assumption of a $\pi i_{13/2}$ assignment. Note that a $\pi h_{9/2}$ assignment cannot be ruled out (see text for details). The excitation energy of each band is referred to in parentheses as E_{ex}. * taken from Ref. [28].

Band 1 ($E_{\text{ex}} = 0$)		Band 2 ($E_{\text{ex}} = 32$ keV*)	
E_γ (keV)	$I^\pi_i \rightarrow I^\pi_f$ ($\hbar$)	E_γ (keV)	$I^\pi_i \rightarrow I^\pi_f$ ($\hbar$)
78*	$9/2^+ \rightarrow 5/2^+$	101*	$11/2^+ \rightarrow 7/2^+$
127.1	$13/2^+ \rightarrow 9/2^+$	143.4	$15/2^+ \rightarrow 11/2^+$
153.7	$17/2^+ \rightarrow 13/2^+$	186.6	$19/2^+ \rightarrow 15/2^+$
200.5	$21/2^+ \rightarrow 17/2^+$	227.4	$23/2^+ \rightarrow 19/2^+$
245.9	$25/2^+ \rightarrow 21/2^+$	265.7	$27/2^+ \rightarrow 23/2^+$
282.6	$29/2^+ \rightarrow 25/2^+$	300.0	$31/2^+ \rightarrow 27/2^+$
316.4	$33/2^+ \rightarrow 29/2^+$	331.9	$35/2^+ \rightarrow 31/2^+$
346.3	$37/2^+ \rightarrow 33/2^+$	360.4	$39/2^+ \rightarrow 35/2^+$
372.4	$41/2^+ \rightarrow 37/2^+$	387.8	$43/2^+ \rightarrow 39/2^+$
402.4	$45/2^+ \rightarrow 41/2^+$	414.9	$47/2^+ \rightarrow 43/2^+$
425.3	$49/2^+ \rightarrow 45/2^+$	(439.5)	$(51/2^+) \rightarrow 47/2^+$
(449.4)	$(53/2^+) \rightarrow 49/2^+$		

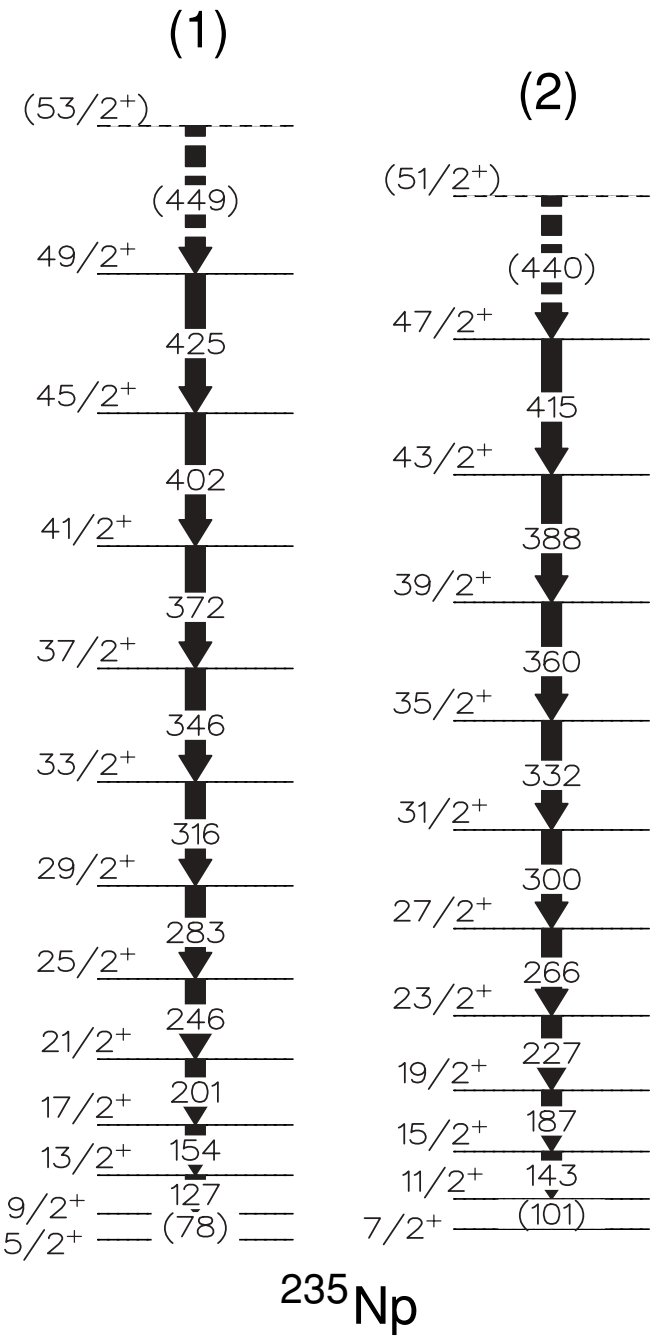

FIG. 5. Proposed level scheme for ^{235}Np deduced in this work. The energies of the γ-ray transitions are given in keV. Transitions and states for which the assignment should be considered tentative are given in parentheses. Note that this scheme assumes that the $\pi i_{13/2}$ configuration is observed; however, a $\pi h_{9/2}$ configuration cannot be ruled out (see text for details).

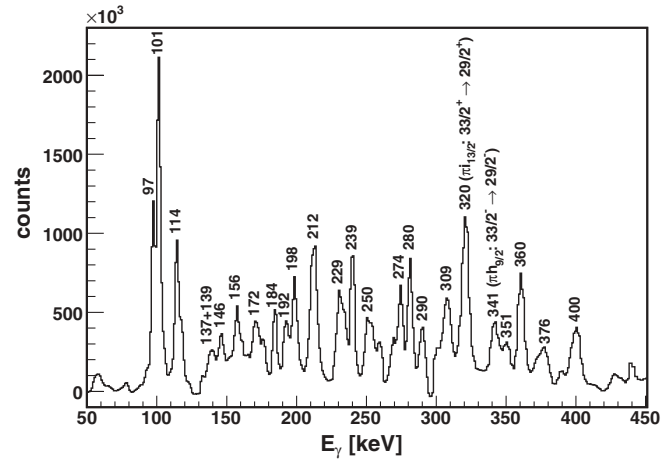

FIG. 6. Coincidence γ-γ-γ projection of γ rays Doppler corrected for neptunium. Strong transitions evident in ^{237}Np [20] are clearly identified and labeled, in addition to the X rays belonging to neptunium. The $33/2 \rightarrow 29/2$ transitions discussed in the text are marked appropriately.

could be easily separated, with transitions at 320 and 341 keV for the $i_{13/2}$- and $h_{9/2}$-based configurations, respectively, and thus reliable intensity measurements could be extracted. Only $\sim$30(1)% of this summed transition intensity is attributed to the $33/2^- \rightarrow 29/2^-$ transition in the excited quasiproton $h_{9/2}$ band. Furthermore, a comparison of the ratios of the γ-ray yields observed in this work for signature $2n$-transfer transitions in ^{118}Sn and ^{235}Np relative to the corresponding inelastic transitions [i.e., $\frac{N_\gamma(^{118}\mathrm{Sn};2_1^+\rightarrow 0^+_{\mathrm{g.s.}})}{N_\gamma(^{116}\mathrm{Sn};2_1^+\rightarrow 0^+_{\mathrm{g.s.}})} = 0.0382(5)$ and the normalized ratio for the corresponding $\pi i_{13/2}$ in-band transitions $\frac{N_\gamma(^{235}\mathrm{Np};35/2^+\rightarrow 31/2^+)}{N_\gamma(^{237}\mathrm{Np};35/2^+\rightarrow 31/2^+)} \times 0.70(1) = 0.0347(52)$] implies that $\sim$70% of the $2n$-transfer cross section proceeds directly to the ground-state band in ^{235}Np, assuming similar neutron-transfer spectroscopic factors for $i_{13/2}$ and $h_{9/2}$ bands. This would, therefore, suggest a $[642]5/2^+$ Nilsson configuration of $i_{13/2}$ parentage as the most likely ground-state assignment upon which the observed rotational sequences in ^{235}Np, bands 1 and 2, are built. This observation and subsequent assignment concur with a previous study by Friedman *et al.* [28], where it was found that nearly the entire $2n$-transfer cross section directly populated the $5/2^+$ ground state in ^{235}Np using a ^{237}Np(p,t) reaction.

A representative coincidence spectrum for band 1 of ^{235}Np is presented in Fig. 7(a). This spectrum is a sum of all double coincidence gates placed on transitions in the 246–316 keV cascade in coincidence with the 346-keV transition in the same sequence. An energy resolution of $\sim$1.0% could be achieved at a γ-ray energy of 316 keV. Ten new transitions above the $13/2^+$ state have been identified in this rotational sequence. In addition, neptunium-like X rays at 97, 101, and 114 keV are also clearly visible in the spectrum, thus confirming the association of the observed γ rays with ^{235}Np. Systematic comparisons with earlier work in ^{237}Np [19,20] suggest that the transitions associated with band 1 are built on top of the $5/2^+$ ground state in ^{235}Np [28,29]. Although there is no firm evidence for the two lowest members of the cascade, due to overwhelming internal conversion at these energies, both states have been identified in previous work [28,29] and systematics would imply their inclusion as shown in Fig. 5. It should be noted that our transition energy at 127(1) keV, for the $13/2^+ \rightarrow 9/2^+$ transition in band 1, deviates slightly from the suggested mean value of 124(3) keV in the previous work of Friedman *et al.* [28]. However, the two suggested

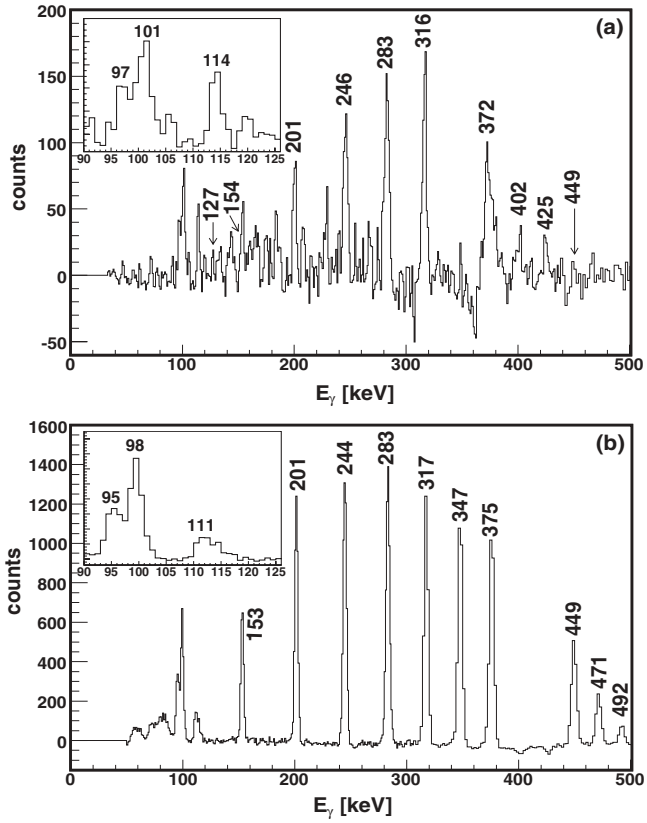

FIG. 7. (a) Representative coincidence γ-ray energy spectrum for the $\alpha = +1/2$ signature partner (band 1) of the observed band in ^{235}Np. The spectrum is the result of a sum of all double coincidence gates placed on transitions in the 246–316 keV sequence in coincidence with the 346-keV transition from the same cascade. The inset provides an expanded low-energy region around the signature neptunium X rays. (b) A coincidence spectrum from an earlier measurement using the reaction ^{234}U(^{209}Bi,^{209}Bi)^{234}U* [30]. This spectrum is the result of all γ rays in coincidence with both the 401- and 426-keV transitions in ^{234}U. The inset shows an expanded low-energy region around the signature uranium X rays.

transition energies are within one standard deviation of one another. Using j mod 2, band 1 is assigned as the $\alpha = +1/2$ signature partner of the ground-state band in ^{235}Np. It should be noted that the sequence of excited states assigned to band 1 in ^{235}Np ($N = 142$) is very nearly degenerate with members of the ground-state band in the neighboring isotone ^{234}U [12]. The ground-state band of ^{234}U populated in the inelastic channel from a previous Gammasphere/CHICO experiment using the reaction 0.3 mg/cm^2 ^{234}U + 1450-MeV ^{209}Bi [30] is presented in Fig. 7(b). Although the transition energies are nearly identical in most cases (notable exceptions are the 246- and 372-keV transitions in ^{235}Np; cf. the 244- and 375-keV transitions in ^{234}U), the X-ray analysis confirms the association of the different chemical elements in each case. Indeed, uranium X-ray lines at 95, 98, and 111 keV are observed in Fig. 7(b), thus confirming the association with ^{234}U in this case.

Similarly, representative coincidence spectra are presented in Fig. 8, which verify the proposed sequence of excited states for band 2 from Fig. 5. The spectrum of Fig. 8(a) represents the sum of all double coincidence gates placed on transitions in the 187–388 keV cascade (apart from the 300-keV transition) in coincidence with the 300-keV transition, while a spectrum showing the sum of all double coincidence gates placed on transitions in the 227–415 keV cascade (apart from the 266-keV transition) in coincidence with the 266-keV transition is given in Fig. 8(b). Ten new transitions above the $11/2^+$ state have been identified in this work, while the lowest member of the band was established from earlier work described in Refs. [28,29]. Additionally, the observed X rays confirm the association with neptunium. Band 2 has been assigned as the $\alpha = -1/2$ signature partner of the ^{235}Np ground-state rotational sequence.

IV. DISCUSSION

The experimental results for ^{235}Np are discussed here in comparison with neighboring nuclei in the region. As

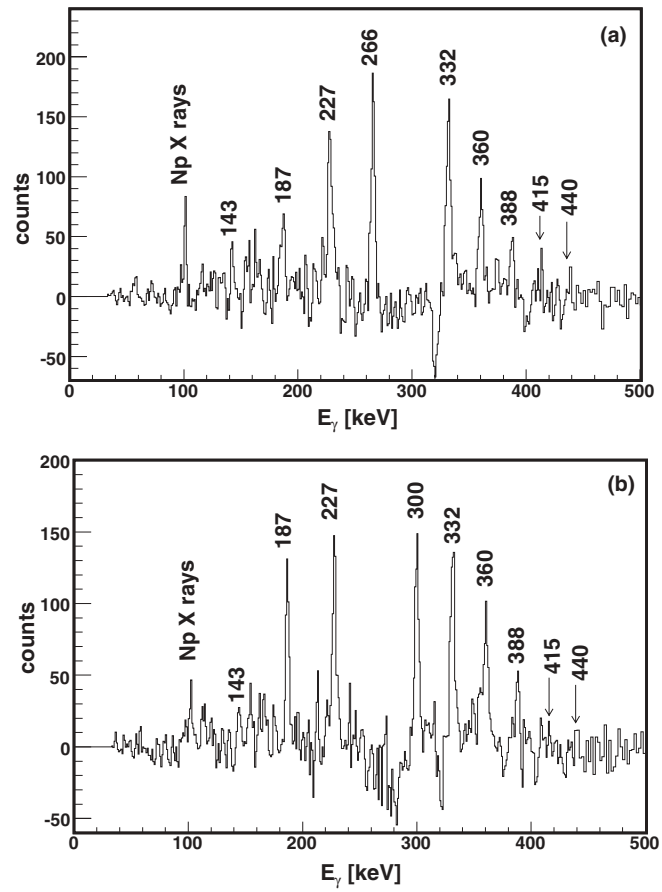

FIG. 8. Representative coincidence γ-ray energy spectra revealing the $\alpha = -1/2$ signature partner (band 2) of the observed band in ^{235}Np. (a) The result of a sum of all double coincidence gates placed on transitions in the 187–388 keV sequence in coincidence with the 300-keV transition from the same cascade. (b) The result of a sum of all double coincidence gates placed on transitions in the 227–415 keV sequence in coincidence with the 266-keV transition from the same cascade.

mentioned in Sec. III, the most favorable mechanism for the $2n$-transfer reaction proceeds directly from the $\pi i_{13/2}$ ground state in ^{237}Np to the ground state in ^{235}Np. Orbital angular momentum matching criteria and the large overlap of wave functions for structurally-similar states implies the band populated in ^{235}Np to also be of $\pi i_{13/2}$ parentage. However, an alternative—albeit less probable—mechanism could ensue via the excited quasiproton $h_{9/2}$ state in ^{237}Np. In this case, the $2n$-transfer process would populate a $\pi h_{9/2}$ band in ^{235}Np. In the following discussion, contrasting behavior in the alignment mechanisms, moments of inertia, and the observed degree of signature splitting for nuclei in the region show that both configurations are plausible interpretations for the observed band in ^{235}Np. These results are also discussed in the framework of CSM calculations.

A. Alignment mechanisms in ^{235,237}Np

Even though the underlying quasiparticle configurations for many of the actinides in the deformed U-Pu region have been well established, the observed alignment characteristics for certain nuclei in this region remain a puzzle. One outstanding issue is the lack of firm evidence for $\nu j_{15/2}$ pairs decoupling and contributing significantly to any observed alignment process. A comparison of the high-spin properties of neighboring odd-A nuclei ^{241}Am [20], ^{237}Np [19,20], and ^{235}U [19] with ^{235}Np provides further insight into the role played by the $j_{15/2}$ neutrons in alignment mechanisms in the actinide region.

The alignment as a function of rotational frequency for both signature partners of the $i_{13/2}$ yrast configurations in ^{235,237}Np and the excited $i_{13/2}$ quasiproton band in ^{241}Am are compared in Fig. 9(a). The degree of alignment $i_x(\omega)$ was calculated according to

$$i_x(\omega) = I_x(I) - I_{\rm ref}, \tag{1}$$

where

$$I_x(I) = \sqrt{I(I+1) - K^2}, \tag{2}$$

and

$$I_{\rm ref} = J_0\omega + J_1\omega^3. \tag{3}$$

The same Harris parameters [32] used in Ref. [20], $J_0 = 65\,\mathrm{MeV}^{-1}\hbar^2$ and $J_1 = 365\,\mathrm{MeV}^{-3}\hbar^4$, have also been adopted in this work. In a rotational band, the frequency ω connects states which differ by 2 $\hbar$. Thus, the correct spin associated with ω is I, where $I+1$ is the upper spin and $I-1$ is the lower spin connected by the γ ray. Since ω as a function of I is determined by

$$\omega(I) = \frac{E_\gamma}{I_{x_i}(I) - I_{x_f}(I)}, \tag{4}$$

and given that $I_{x_i}(I) = \sqrt{(I+1)(I+2) - K^2}$, and $I_{x_f}(I) = \sqrt{(I-1)I - K^2}$, it therefore follows that $\omega(I) \approx E_\gamma/2$. Figure 9(a) indicates approximately equal initial alignments of $1.2 \sim 1.4$ $\hbar$ for all three nuclei. Further inspection of this plot shows that the alignment of the ground-state band in ^{237}Np, based on a $[642]5/2^+$ ($\pi i_{13/2}$) Nilsson configuration, gradually increases with

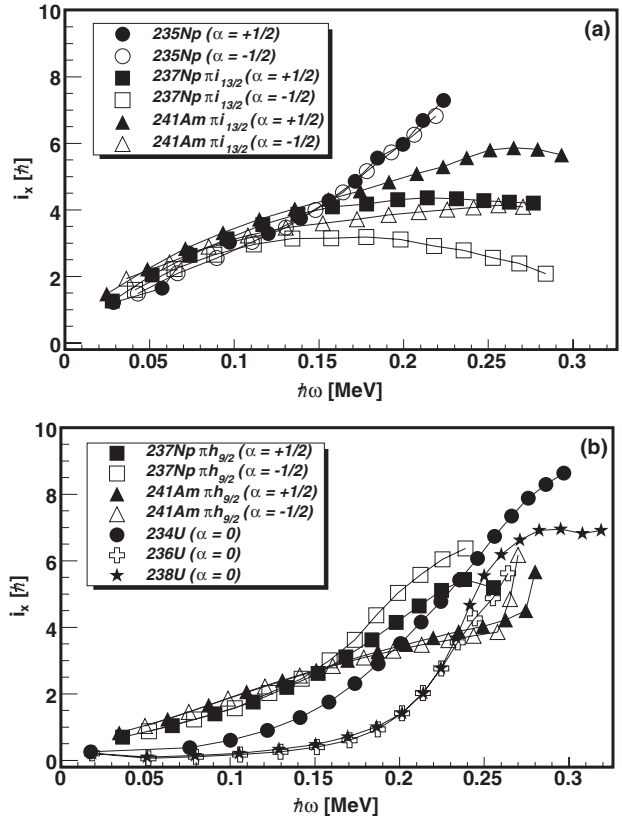

FIG. 9. Aligned angular momentum as a function of rotational frequency for (a) the $\pi i_{13/2}$ $[642]5/2^+$ bands in ^{237}Np (ground state) and ^{241}Am (excited quasiproton), and the observed band in ^{235}Np and (b) the $\pi h_{9/2}$ $[523]5/2^-$ bands in ^{237}Np (excited quasiproton) and ^{241}Am (ground state) and the yrast ($\alpha = 0$) bands in the even-even nuclei ^{234}U [12,30], ^{236}U [12], and ^{238}U [11,31]. For all data points, a reference configuration with the Harris parameters [32] $J_0 = 65\,\mathrm{MeV}^{-1}\hbar^2$ and $J_1 = 365\,\mathrm{MeV}^{-3}\hbar^4$ has been subtracted.

rotational frequency up until $\hbar\omega \sim 0.11$ MeV. At this point, the alignment tends to saturate: first in the $\alpha = -1/2$ signature partner; later in the $\alpha = +1/2$ signature. The excited $i_{13/2}$-quasiproton band in ^{241}Am generally displays a behavioral pattern similar to ^{237}Np, although it has a greater gain in alignment over the observed frequency range. The signature partners of the yrast band in ^{235}Np mimic the behavior of that observed in ^{237}Np and ^{241}Am up to a rotational frequency of $\hbar\omega \sim 0.14$ MeV, at which point the alignment of the ^{235}Np band continues to rise sharply with increasing rotational frequency rather than saturate. This upbend feature is suggestive of a strong interaction, interpreted as a band crossing, between an aligned s band and a paired configuration, the ground band (g band) [2].

To understand this anomalous behavior in ^{235}Np, it is necessary to compare with systematics of other neighboring nuclei in the region. In Refs. [19,20], a comparison of the alignment properties in ^{235}U, ^{237}Np, and ^{241}Am demonstrated the dominant role of the $i_{13/2}$ protons in the alignment properties observed in this region. As illustrated in Fig. 9(a), a gradual alignment followed by a subsequent saturation in the $i_{13/2}$-based ground-state configuration in ^{237}Np and

excited-quasiproton configuration in ^{241}Am is in sharp contrast to the $\alpha = 0$ yrast bands of ^{234,236,238}U [11,12,30,31] and the $h_{9/2}$ negative-parity bands in ^{237}Np and ^{241}Am (both based on a $\pi h_{9/2}$ [523]5/2$^-$ Nilsson configuration [20]), which all show an onset of alignment, but at varying frequencies [see Fig. 9(b)]. The ^{236,238}U [11,12,31] and ^{237}Np [20] bands in Fig. 9(b) all experience a band crossing at ∼0.2 MeV, at about the same frequency as the first upbend observed in ^{235}U [19,33], and is, hence, likely to be caused by the first $i_{13/2}$ proton alignment. In the case of ^{241}Am, both signature partners of the $h_{9/2}$ band begin to upbend sharply at $\hbar\omega \sim 0.26$ MeV, mimicking the $\pi i_{13/2}$ alignment observed in ^{242}Pu [10,14], and is, therefore, also suggestive of an $i_{13/2}$ proton alignment in ^{241}Am. The lack of any upbend in the $i_{13/2}$ proton bands of ^{237}Np and ^{241}Am indicates either a delay in the crossing frequency or a complete absence of aligning $j_{15/2}$ quasiparticle pairs in the deformed U-Pu region. This conclusion is reinforced by the alignment plots in Fig. 9(b), which show that the observed upbends display similar overall alignment gains of $6 \sim 7\,\hbar$ at their observational limits (with the exception of ^{234}U). Indeed, the near-constant alignment from both signature partners of ^{237}Np in Fig. 9(a) combine to give a total alignment of $\sim 7\,\hbar$, leaving little room to argue for a second pair of aligning quasiparticles in the upbends observed in these nuclei. It is also worth mentioning that several groups have performed independent sets of microscopic calculations [34–36] to study the alignment mechanisms in this region of the actinides. Their results support the experimental conjecture of a broken pair of $i_{13/2}$ protons—and their subsequent alignment with the rotation axis of the core—as the dominant factor explaining the observed upbending effects in this region.

In contrast to the behavior observed for $N = 144$ and 146 for the $\pi i_{13/2}$ bands in ^{237}Np and ^{241}Am, the ^{235}Np bands plotted in Fig. 9(a) clearly show the effects of an aligning pair of quasiparticles. With the $i_{13/2}$ proton crossing blocked by the configuration, the observed upbend would be indicative of a strong interaction between an aligned pair of $j_{15/2}$ neutrons and the $i_{13/2}$ proton orbital upon which the observed rotational band is built in ^{235}Np. This purported scenario provides the first evidence for a strong interaction from the $j_{15/2}$ neutrons in the deformed U-Pu region. It is interesting to note that the yrast band in ^{234}U ($N = 142$) begins to align at ∼0.1 MeV, while the same bands in ^{236,238}U do not begin to align until ∼0.14 MeV, and it undergoes a greater degree of alignment, $\sim 9\,\hbar$, at the observational limit. In light of the new data on ^{235}Np, this early onset and extra alignment observed in ^{234}U [12,30] is likely to come from the $j_{15/2}$ neutrons.

To obtain a better—though qualitative—understanding of the experimental information, sample results of the CSM calculations for $Z = 93$ and $N = 142$ and 144 are presented in Fig. 10. These calculations were performed using the Warsaw-Lund code, which uses a Woods-Saxon potential [37] with the universal parameters given in Ref. [38]. Realistic input values of 0.20 and 0.10 were derived for the deformation parameters β_2 and β_4, respectively, from the corrected earlier $B(E2; 5/2^+_{\text{g.s.}} \rightarrow 7/2^+_1)$ measurement of ^{237}Np [39]. This choice of deformation parameters compares well with those suggested by the potential-energy surface calculations of Ref. [40]. The results of these calculations suggest that

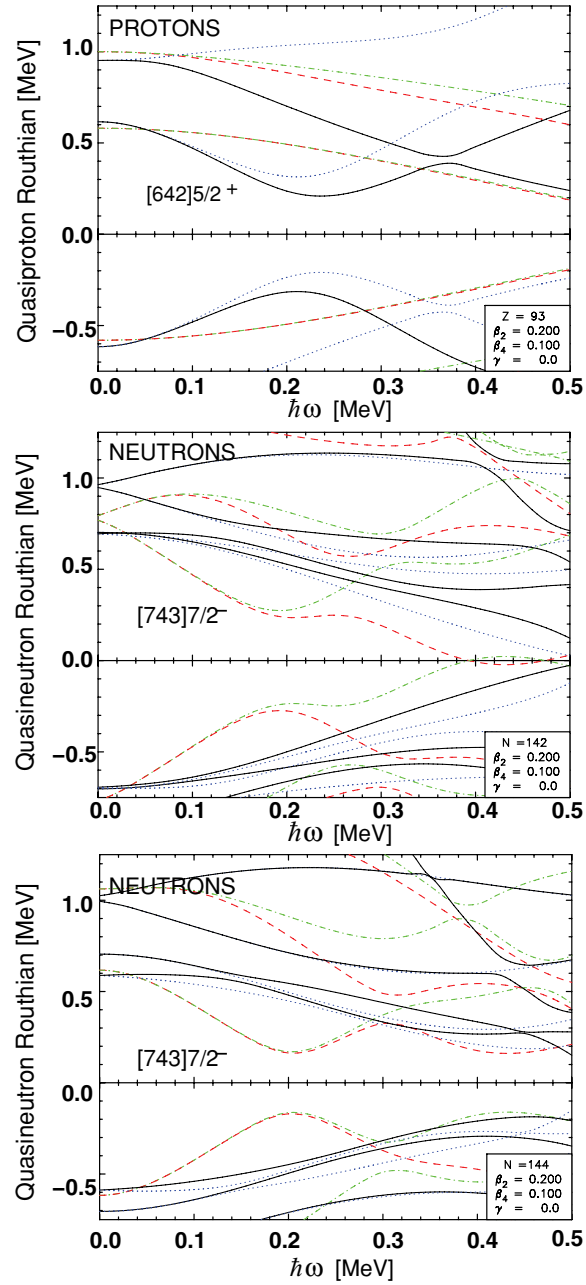

FIG. 10. (Color online) Sample results of the CSM calculations for protons and neutrons corresponding to ^{235}Np ($Z = 93$, $N = 142$) and ^{237}Np ($Z = 93$, $N = 144$). Annotations for the configurations of interest are given just below the actual Routhians. The [642]5/2$^+$ orbital belongs to the $\pi i_{13/2}$ subshell and is predicted to cross the ground band at $\hbar\omega \sim 0.24$ MeV, while the [743]7/2$^-$ orbital belongs to the $\nu j_{15/2}$ subshell and is predicted to cross the ground band at an earlier rotational frequency of $\hbar\omega \sim 0.2$ MeV. See text for further details.

the $j_{15/2}$ neutrons should align first at a crossing frequency of $\hbar\omega \sim 0.2$ MeV, followed by an $i_{13/2}$ proton crossing at $\hbar\omega \sim 0.24$ MeV for both ^{235}Np and ^{237}Np. The calculations also imply a strong interaction from the $j_{15/2}$ neutron orbitals at $N = 142$ and a weaker interaction at $N = 144$, in agreement with the calculations presented in Ref. [15]. Realistic

variations of the β_2 and β_4 deformation parameters do not produce significant changes in the proton and neutron crossing frequencies, with the proton crossing always following the first neutron crossing. Assuming a bandhead based on a $\pi i_{13/2}$ configuration, these results are in good qualitative agreement for describing the placement and interaction strength observed for aligning $j_{15/2}$ neutrons at $N = 142$, but the CSM appears to break down completely for $N = 144$ (as well as $N = 146$ for ^{241}Am) as was pointed out in Ref. [20]. It was suggested in Ref. [20] that the discrepancy between the data and the CSM calculations for $N = 144$ (and $N = 146$) could be due to either a pairing collapse for the neutron system (absence of alignment) or a delay in the expected alignment relative to the calculation. It has also been speculated that enhanced octupole correlations may result in a lower $\nu j_{15/2}$ crossing frequency than expected from the CSM calculations [14,18,20,21]. While the new data do not shed light on either explanation, it does point to a fundamental change in the alignment properties of the $j_{15/2}$ neutrons when going from $N = 142$ to $N = 144$.

It should be noted that the above arguments are predicated on the assumption that the two bands identified are built on the $i_{13/2}[642]5/2^+$ ground-state configuration. If, on the other hand, the two observed bands were built on the $[523]5/2^-$ Nilsson configuration of $h_{9/2}$ parentage whose bandhead lies ~50 keV [29] above the ground state, the observed upbend could be due to the $i_{13/2}$ proton alignment. While this seems unlikely based on arguments presented in Section III, this possibility cannot be ruled out by the available data. This conclusion would also compare well with recent work on neighboring odd-odd nuclei ^{236,238}Np [41] where no evidence has been found for a $\nu j_{15/2}$ alignment.

B. Experimental Routhians

The experimental single-particle Routhians can also be compared with the results of the CSM calculations. The experimental Routhians as a function of rotational frequency for the observed rotational sequences in ^{235}Np are presented in Fig. 11, along with the ground-state and excited-quasiproton bands in ^{237}Np. The Routhian energy $e'(\omega)$ is defined as

$$e'(\omega) = E_{\rm ex} - \hbar\omega(I) I_x(I) - E_{\rm ref}(\omega), \tag{5}$$

where $E_{\rm ex}$ is the *average* excitation energy of a pair of states connected by a single γ-ray transition, and thus gives the correct correlation with I defined earlier as the intermediate spin between a pair of states, and

$$E_{\rm ref}(\omega) = -\left(\frac{J_0\omega^2}{2} + \frac{J_1\omega^4}{4} - \frac{1}{8J_0}\right). \tag{6}$$

The experimental data for ^{237}Np show that the signature splitting, given by the energy difference between a pair of signature partners, for the $\pi i_{13/2}$ $[642]5/2^+$ partners increases gradually with increasing rotational frequency, in good agreement with the CSM calculations presented here in Fig. 10 and in Ref. [20]. The results of the CSM calculations for ^{235}Np in Fig. 10 also show a gradual increase in signature splitting with rotational frequency for the $i_{13/2}$ $[642]5/2^+$ signature partners, in clear contradiction to the experimental data at the current

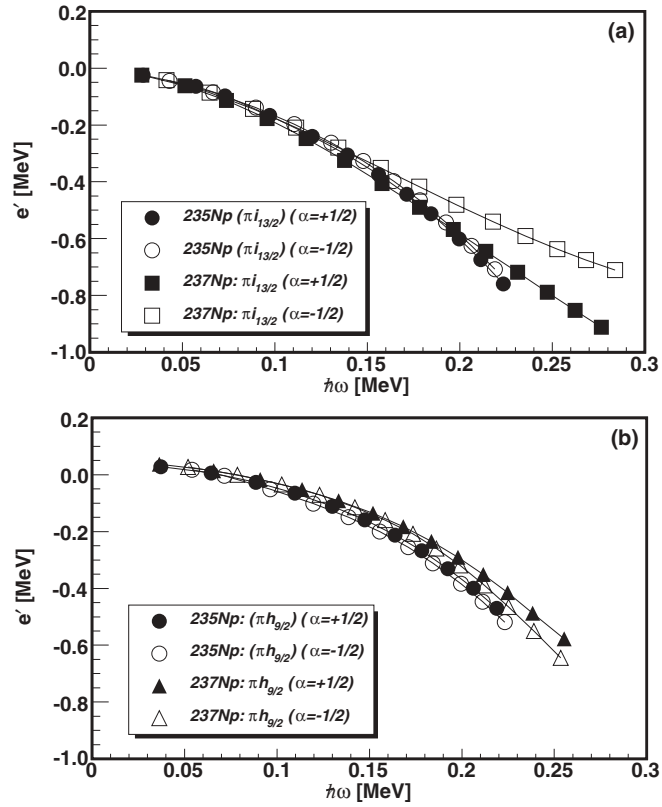

FIG. 11. Routhians as a function of rotational frequency for (a) the ground-state $\pi i_{13/2}$ $[642]5/2^+$ band in ^{237}Np and observed band in ^{235}Np assuming an $i_{13/2}$ configuration, and (b) the excited-quasiproton $\pi h_{9/2}$ $[523]5/2^-$ band in ^{237}Np and the observed band in ^{235}Np assuming an $h_{9/2}$ configuration. For all data points, a reference configuration with the Harris parameters [32] $J_0 = 65\,\text{MeV}^{-1}\hbar^2$ and $J_1 = 365\,\text{MeV}^{-3}\hbar^4$ has been subtracted.

observational limit. Assuming the observed band in ^{235}Np is built on a $\pi i_{13/2}$ configuration, Fig. 11(a) shows that the data for ^{235}Np and the $\pi i_{13/2}$-based ground-state band in ^{237}Np mimic each other rather well at low rotational frequencies, up to $\hbar\omega \sim 0.15$ MeV. At this point, there is a splitting in the Routhians between the two signature partners in ^{237}Np, but not in ^{235}Np. This lack of signature splitting makes it difficult to confirm the assignment of an $i_{13/2}$ configuration for the observed band in ^{235}Np. On the other hand, if a $\pi h_{9/2}$ configuration is assumed (this requires a reversal of the signature quantum numbers and parities of the states belonging to the observed rotational sequences in ^{235}Np), as shown in Fig. 11(b), the calculated Routhians display quite similar behavior to the corresponding Routhians of the $\pi h_{9/2}$ band in ^{237}Np, and over a greater frequency range. However, Fig. 11(b) also shows that the $\pi h_{9/2}$ band in ^{237}Np begins to undergo signature splitting—though to a lesser degree than the $\pi i_{13/2}$ band—at $\hbar\omega \sim 0.18$ MeV, while, again, no signature splitting is observed over the entire frequency range for the corresponding band in ^{235}Np. Thus, it is difficult to establish a firm assignment, $\pi i_{13/2}$ $[642]5/2^+$ or $\pi h_{9/2}$ $[523]5/2^-$, for the observed band in ^{235}Np on the basis of the Routhian data presented here.

It should be noted, however, that the experimental data suggest the observed $\alpha = \pm 1/2$ rotational sequences in ^{235}Np form a strongly-coupled configuration. This can be seen from the coincidence spectra presented in Figs. 7 and 8, which clearly show coincidence relationships between members of both $\alpha = \pm 1/2$ cascades. A strongly-coupled configuration was also observed for the $\pi h_{9/2}$-based rotational sequences in ^{237}Np, but not for the $\pi i_{13/2}$ band, and hence, systematics would thus imply the observed rotational sequences in ^{235}Np are also built on a $\pi h_{9/2}$ orbital. However, due to the nature of the low-energy $M1$ interband linking transitions, internal-conversion processes, and efficiency limitations, discrete $M1$ transitions between the two signature partners in ^{235}Np cannot be positively identified. Under these circumstances, it has not been possible to extract $B(M1)/B(E2)$ branching ratios that could otherwise be compared with those expected for $\pi i_{13/2}$ and $\pi h_{9/2}$ configurations and hence lead to an unambiguous assignment for the observed band.

C. Kinematic and dynamic moments of inertia

Further evidence for the contrasting behavior between the two isotopes ^{235}Np and ^{237}Np can be observed from their kinematic and dynamic moments of inertia, illustrated by the plots in Figs. 12(a) and 12(b), respectively. The kinematic moment of inertia $J^{(1)}$ was calculated according to

$$J^{(1)} = \frac{\hbar^2}{E_\gamma}(2I - 1), \tag{7}$$

while the dynamic moment of inertia $J^{(2)}$, which depends only on the transition energy, was extracted using

$$J^{(2)} = \frac{4\hbar^2}{\Delta E_\gamma}. \tag{8}$$

These moment-of-inertia plots readily illustrate structural differences between bands. The ground-state $i_{13/2}$ signature partners belonging to ^{237}Np exhibit a near-constant kinematic moment of inertia over the observed frequency range [Fig. 12(a)], with the favored $\alpha = +1/2$ partner having the larger $J^{(1)}$ value. The $h_{9/2}$ quasiproton signature partners, on the other hand, reveal a gradual increase in $J^{(1)}$ with increasing rotational frequency up to $\hbar\omega \sim 0.16$ MeV, at which point the $J^{(1)}$ values for the two sequences deviate from each other. Above this frequency, both sequences experience a much steeper increase, with the unfavored $\alpha = -1/2$ signature partner showing the steepest. The observed upbend in $J^{(1)}$ with increasing rotational frequency is suggestive of an alignment of $i_{13/2}$ protons. The data for ^{235}Np, according to the signature and spin assignments corresponding to the level scheme presented in Fig. 5, track closely the near-constant $J^{(1)}$ moment observed in the $i_{13/2}$ band of ^{237}Np at lower rotational frequencies. Around $\hbar\omega \sim 0.14$ MeV, $J^{(1)}$ values start to increase rapidly in a manner akin to that of the $h_{9/2}$ sequences in ^{237}Np. This upbend in $J^{(1)}$ coincides with the alignment frequency in Fig. 9(a), where the ^{235}Np band upbends (cf. the $i_{13/2}$ bands in ^{237}Np and ^{241}Am) and could indicate a strong interaction arising from the candidate $j_{15/2}$ neutron orbitals. This would support a ground-state configuration $\pi i_{13/2}$ [642]5/2$^+$ for the

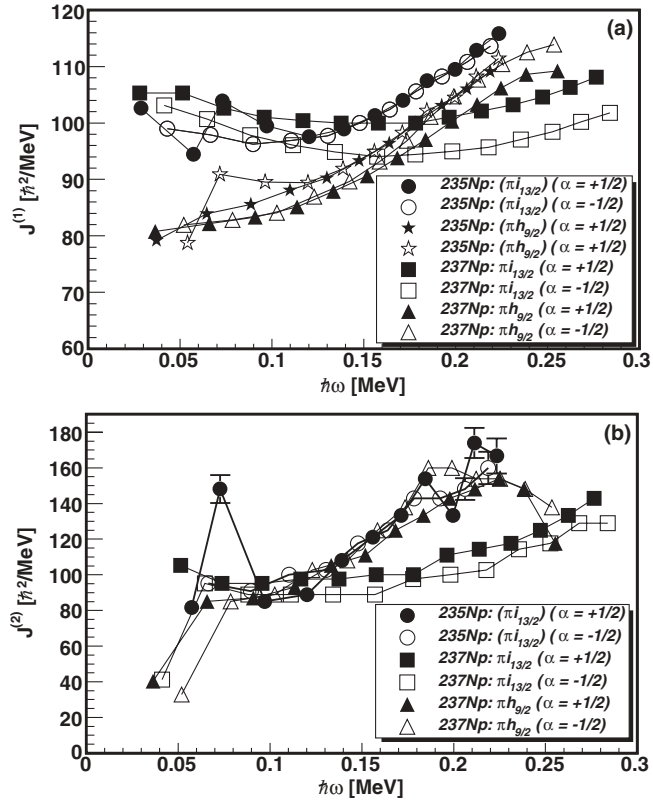

FIG. 12. (a) Kinematic moment of inertia as a function of rotational frequency for the ground-state $i_{13/2}$ [642]5/2$^+$ and excited-quasiproton $h_{9/2}$ [523]5/2$^-$ signature partners in ^{237}Np, in addition to both postulated assignments ($i_{13/2}$ and $h_{9/2}$) for the observed bands in ^{235}Np. (b) Dynamic moment of inertia as a function of rotational frequency for the ground-state $i_{13/2}$ [642]5/2$^+$ and excited-quasiproton $h_{9/2}$ [523]5/2$^-$ signature partners in ^{237}Np, in addition to the observed bands in ^{235}Np.

observed band in ^{235}Np. On the other hand, if the signature quantum numbers for the observed bands in ^{235}Np were to be reversed and assuming they are built on a $\pi h_{9/2}$ [523]5/2$^-$ configuration, then the $J^{(1)}$ values for ^{235}Np mimic very closely those observed in the $h_{9/2}$ band of ^{237}Np as shown by the alternative postulated assignment for the ^{235}Np sequences in Fig. 12(a). This scenario would, therefore, favor a strong interaction from the $i_{13/2}$ protons with little to no contribution from the $j_{15/2}$ neutrons. However, it should also be noted that the $J^{(1)}$ moments for assumed $h_{9/2}$ rotational sequences in ^{235}Np do not deviate from one another, quite unlike what is observed in ^{237}Np. In view of the fact that these bands have transition energies that are so similar, it has thus been demonstrated that the configuration cannot be established on the basis of the $J^{(1)}$ moments alone.

The dynamic moment of inertia can also be instructive, since it is a derivative of the kinematic moment of inertia and, therefore, sensitive to even very small structural changes. Unfortunately, the $J^{(2)}$ moments also fail to pin down a unique configuration for the observed signature partners in ^{235}Np. As can be seen from Fig. 12(b), with the exception of the oscillations at the beginning of the bands, the $J^{(2)}$ moments for all bands are fairly similar. The ^{235}Np bands (regardless of

signature and parity assignments) and the $h_{9/2}$-based ^{237}Np bands then begin to deviate from the $i_{13/2}$ ^{237}Np bands once the band crossings set in. Consequently, these results merely show that these bands at low spin are very similar in their transition energies regardless of configuration, while at high-spin, the deviations are due to band crossings. Again, these results invoke both possibilities for either a $[642]5/2^+$ or $[523]5/2^-$ configuration originating from the $i_{13/2}$ and $h_{9/2}$ proton subshells, respectively, for the observed band in ^{235}Np. Hence, none of the physical quantities extracted from the present ^{235}Np experiment lead to an unambiguous orbital assignment.

V. SUMMARY

The $j_{15/2}$ neutron orbitals have the highest orbital-angular momentum ($l = 7$) available for studying issues related to rotational alignment and thus provide a stringent test of the CSM. The optimum case for studying this issue is ^{235}Np, since nuclei in the transuranic region with $N = 142$ are predicted by the CSM to exhibit the strongest interaction between rotationally-aligned paired and ground-state bands [6]. Furthermore, a $\pi i_{13/2}$ ground-state band blocks the possible alignment due to the $i_{13/2}$ proton orbitals, bringing into play the possible role of the $j_{15/2}$ neutron orbitals to explain candidate alignment effects.

The level scheme for ^{235}Np has been delineated to high spin for the first time using a heavy-ion induced $2n$-transfer reaction. Two rotational sequences have been unambiguously assigned to ^{235}Np through a cross correlation of the γ rays of interest with those corresponding to the $2n$-transfer partner ^{118}Sn. The alignment properties, Routhians, and moments of inertia for the observed rotational sequences support the assertion that the observed structures are, in fact, signature partners. A measurement of the γ-ray yields between the $2n$-transfer and inelastic reaction channels shows that nearly the entire $2n$-transfer cross section is exhausted through the population of the ground-state band, in agreement with a previous (p, t) transfer measurement [28]. This would imply that the observed rotational sequences in ^{235}Np are the signature partners of the ground-state band built on a $[642]5/2^+$ Nilsson orbital of $\pi i_{13/2}$ parentage. The favored $\alpha = +1/2$ and unfavored $\alpha = -1/2$ rotational sequences have been populated to $49/2^+$ $\hbar$ (tentatively to $53/2^+$ $\hbar$) and $47/2^+$ $\hbar$ (tentatively to $51/2^+$ $\hbar$), respectively. It is interesting to note that the $\alpha = +1/2$ rotational sequence of the observed band in ^{235}Np ($N = 142$) is nearly degenerate with the yrast band in its isotonic even-even neighbor ^{234}U [12]. Such observations are frequently encountered in the actinides [27].

The alignment mechanism for the observed band in ^{235}Np is clearly very different from that of the proton-blocked $i_{13/2}$ bands in neighboring odd-A nuclei ^{237}Np and ^{241}Am; a saturation of the alignment is observed in ^{237}Np and ^{241}Am, whereas ^{235}Np exhibits a clear upbend. Since the $\pi i_{13/2}$ orbital is blocked in the case of ^{235}Np, this upbend is likely to be attributed to a strong interaction between an aligned pair of $j_{15/2}$ neutrons and the $i_{13/2}$ ground state built on a $[642]5/2^+$ proton orbital. The near-constant and upbending $J^{(1)}$ moments for the ground-state band in ^{237}Np ($\pi i_{13/2}$) and the assumed $\pi i_{13/2}$-based band in ^{235}Np, respectively, support this suggestion. However, the same quantity also supports a $\pi h_{9/2}$ configuration upon reversing the signature and parity assignments for the observed ^{235}Np rotational sequences. The CSM calculations also attribute the first alignment to a broken pair of $j_{15/2}$ neutrons from the $[743]7/2^-$ Nilsson orbital. Thus, while there is evidence to demonstrate the moderate role played by the $j_{15/2}$ neutrons in the transuranic region, e.g., the gradual alignment observed at low spin in ^{248}Cm [13], and in the transfermium region [42], this work may well provide the first evidence for $\nu j_{15/2}$ dominance in the deformed U-Pu region. However, it cannot be overlooked that a less probable reaction mechanism could lead to the population of a quasiproton band in ^{235}Np based on a $[523]5/2^-$ Nilsson orbital of the $\pi h_{9/2}$ subshell. In this case, the first alignment is likely to be attributed to a broken pair of $i_{13/2}$ protons. Furthermore, the lack of any signature splitting up to the observational limit and the similarities between the $J^{(2)}$ moments for the observed band in ^{235}Np and the excited $h_{9/2}$ quasiproton band in ^{237}Np make it impossible to completely rule out a negative-parity assignment for the observed band.

ACKNOWLEDGMENTS

This work was performed under the auspices of the US Department of Energy by Lawrence Livermore National Laboratory under Contract DE-AC52-07NA27344. Work at Argonne National Laboratory is supported by the US Department of Energy, Office of Nuclear Physics, under Contract DE-AC02-06CH11357. Further support was provided by the US Air Force Office of Scientific Research, the National Science Foundation, and the Science and Technology Facilities Council of the United Kingdom.

[1] D. R. Inglis, Phys. Rev. **96**, 1059 (1954).
[2] F. S. Stephens and R. S. Simon, Nucl. Phys. **A183**, 257 (1972).
[3] S. Frauendorf, Phys. Scr. **24**, 349 (1981).
[4] B. R. Mottelson and J. G. Valatin, Phys. Rev. Lett. **5**, 511 (1960).
[5] R. Bengtsson, I. Hamamoto, and B. Mottelson, Phys. Lett. **B73**, 259 (1978).
[6] Y. S. Chen and S. Frauendorf, Nucl. Phys. **A393**, 135 (1983).
[7] O. Häusser *et al.*, Phys. Rev. Lett. **48**, 383 (1982).
[8] R. S. Simon, R. P. Devito, H. Emling, R. Kulessa, C. Briançon, and A. Lefebvre, Phys. Lett. **B108**, 87 (1982).
[9] E. Grosse *et al.*, Phys. Scr. **24**, 337 (1981).
[10] W. Spreng *et al.*, Phys. Rev. Lett. **51**, 1522 (1983).
[11] D. Ward *et al.*, Nucl. Phys. **A600**, 88 (1996).
[12] H. Ower *et al.*, Nucl. Phys. **A388**, 421 (1982).
[13] R. B. Piercey *et al.*, Phys. Rev. Lett. **46**, 415 (1981).
[14] I. Wiedenhöver *et al.*, Phys. Rev. Lett. **83**, 2143 (1999).
[15] J. Dudek, W. Nazarewicz, and Z. Szymanski, Phys. Scr. **T5**, 171 (1983).
[16] J. L. Egido and P. Ring, Nucl. Phys. **A423**, 93 (1984).
[17] R. K. Sheline and M. A. Riley, Phys. Rev. C **61**, 057301 (2000).

[18] X. Wang *et al.*, Phys. Rev. Lett. **102**, 122501 (2009).
[19] R. Kulessa *et al.*, Z. Phys. A **312**, 135 (1983).
[20] K. Abu Saleem *et al.*, Phys. Rev. C **70**, 024310 (2004).
[21] S. Zhu *et al.*, Phys. Lett. **B618**, 51 (2005).
[22] I. Y. Lee, Nucl. Phys. **A520**, 641c (1990).
[23] M. W. Simon, D. Cline, C. Y. Wu, R. W. Gray, R. Teng, and C. Long, Nucl. Instrum. Methods Phys. Res. A **452**, 205 (2000).
[24] ROOT: An object-oriented data analysis framework, http://root.cern.ch/.
[25] D. C. Radford, Nucl. Instrum. Methods Phys. Res. A **361**, 306 (1995).
[26] C. Y. Wu, W. von Oertzen, D. Cline, and M. W. Guidry, Annu. Rev. Nucl. Part. Sci. **40**, 285 (1990).
[27] I. Ahmad, M. P. Carpenter, R. R. Chasman, R. V. F. Janssens, and T. L. Khoo, Phys. Rev. C **44**, 1204 (1991).
[28] A. M. Friedman, K. Katori, D. Albright, and J. P. Schiffer, Phys. Rev. C **9**, 760 (1974).
[29] R. D. Griffioen, R. C. Thompson, and J. R. Huizenga, Phys. Rev. C **18**, 671 (1978).
[30] C. Y. Wu *et al.* (unpublished).
[31] M. W. Simon, D. Cline, C. Y. Wu, R. Teng, K. Vetter, and A. O. Macchiavelli (unpublished).
[32] S. M. Harris, Phys. Rev. **138**, B509 (1965).
[33] J. de Bettencourt, C. Briançon, J. Libert, J. P. Thibaud, R. J. Walen, A. Gizon, M. Meyer, and P. Quentin, Phys. Rev. C **34**, 1706 (1986).
[34] J. L. Egido and P. Ring, J. Phys. G **8**, L43 (1982).
[35] M. Diebel and U. Mosel, Z. Phys. A **303**, 131 (1981).
[36] M. Ploszajczak and A. Faessler, J. Phys. G **8**, 709 (1982).
[37] W. Nazarewicz, J. Dudek, R. Bengtsson, T. Bengtsson, and I. Ragnarsson, Nucl. Phys. **A435**, 397 (1985).
[38] J. Dudek, Z. Szymanski, and T. Werner, Phys. Rev. C **23**, 920 (1981).
[39] J. O. Newton, Nucl. Phys. **5**, 218 (1958).
[40] A. Sobiczewski, I. Muntian, and Z. Patyk, Phys. Rev. C **63**, 034306 (2001).
[41] M. P. Carpenter *et al.* (unpublished).
[42] R.-D. Herzberg and P. T. Greenlees, Prog. Part. Nucl. Phys. **61**, 674 (2008).